Available online at www.sciencedirect.com
SCIENCE DIRECT®
Journal of Theoretical Biology 226 (2004) 483–501
Journal of Theoretical Biology
www.elsevier.com/locate/jtbi

Modeling threshold phenomena, metabolic pathways switches and signals in chemostat-cultivated cells: the Crabtree effect in *Saccharomyces cerevisiae* ☆

Jacques Thierie*

Université Libre de Bruxelles, Faculté des Sciences, Section interfacultaire d'Agronomie, Laboratoire de Physiologie et Ecolgie microbiennes (UPEM), Faculté des Sciences-Ecole interfacultaire des bioingénieurs, Laboratoire de Physiologie et Ecologie microbiennes (UPEM), c/o Institute Pasteur, 642, rue Engeland, Brussels 1080, Belgium

Received 9 October 2002; received in revised form 25 July 2003; accepted 23 October 2003

Abstract

The long-term Crabtree effect in *Saccharomyces cerevisiae* cultivated in aerobic chemostat at steady state has been studied for three different substrate concentrations in the feed of the bioreactor (data: J. Gen. Microbiol., 129 (1983) 653). We have shown that a model using two ways of transport/metabolization (T/M) of hyperbolic form, with high and low affinity for the substrate, allowed to represent correctly the main characteristics of the phenomenon. The model is based on an explicit form of the T/M kinetics when the bioreactor is considered as a polyphasic dispersed system (PDS). Mass balances analysis also allows to quantify the critical dilution rate value (threshold), D_c, of the transition between respiratory and respirofermentative mode, for which ethanol is produced. A good approximation for the threshold is $D_c = V_S^0 Y_{X^c,S}$ where $Y_{X^c,S}$ is the average yield coefficient before transition and V_S^0, the maximum specific rate of high affinity T/M pathway. The theoretical value is $0.3\,h^{-1}$, and is equal to the experimental value. We thus show in a quantitative way that the transition depends both on culture conditions (global characteristic of the system) and on strain properties (intrinsic characteristic of the microorganism as well). Using two different methods to calculate the residual substrate has carried out the comparison between the simulations end the experimental data. This allowed showing that the latter is not well represented by Monod's model and has confirmed that the affinity for the substrate varies according to the biomass. We have then shown how to calculate the most important specific rates (or metabolic flux) related to biomass, ethanol, oxygen, hydrogen, respiratory and fermentative CO_2 and H_2O within the cellular phase. It has appeared that the oxygen uptake rate directly depends on high-affinity T/M pathway. This let us think that the regulation of the Crabtree effect in *S. cerevisiae* depends on the saturation of some glucose metabolization and transport pathways rather than on saturation of the respiratory chains. The specific rates analysis has also allowed us to show, at least in this case, that the metabolization rate (biosynthesis + fueling) had its maximum value on the whole dilution rates interval; metabolites excretion (ethanol and fermentative CO_2) only intervenes to drain a "surplus" glucose flux. As a consequence, the transport capacity must be higher than the one of metabolization. Maximization of the metabolization specific rate could then be used as an optimization criterion in the stoichiometric calculation of metabolic flux (and not the specific growth rate maximization because growth is limited in a chemostat ($\mu = D$)). We have also shown that the mass balances based on the T/M processes are in agreement with molar and elementary balances of the general stoichiometric equation for glucose respiration and fermentation under aerobic conditions. Thanks to the specific rates calculating the stoichiometric coefficients has done this. The total mass balance difference does not exceed 4%, which is compatible with the experimental carbon balance. Finally, we have emphasized that the ratio of biosynthesis flux and metabolization flux is constant before and after transition. This observation could be applied as soon as the free substrate concentration in the cellular phase is low. The paper succinctly describes the former theoretical results on which the model is built and sufficiently explains the algorithm for straightforward implementation.

Keywords: Polyphasic dispersed systems; Pseudo-homogeneous concentration; Respirofermentative metabolism

1. Introduction

It is well known that the adaptation capacities of micro-organisms are considerable according to modifications in

☆ Supplementary data associated with this article can be found, in the online version doi = 10.1016/j.jtbi.2003.10.017

*Fax: +32-02-373-33-09.
E-mail address: upemulb@resulb.ulb.ac.be (J. Thierie).

0022-5193/$ - see front matter © 2003 Elsevier Ltd. All rights reserved.
doi:10.1016/j.jtbi.2003.10.017

external constraints. However, in a biological system like a chemostat, the majority of the observable macroscopic variables (biomass, substrate concentration, etc) generally change in a continuous way when the environmental constraints also change in a continuous way. There are however remarkable exceptions to this "regular" rule and the long-term Crabtree effect is a good example of it. Phenomenologically, at low dilution rates (D), the yeasts grow with a constant substrate-related yield coefficient and the biomass almost remains relatively constant in the chemostat. The specific oxygen consumption rate increases in a linear way with D, and the substrate metabolism (glucose, for example) is performed in a merely respiratory (or oxidative) way. For some yeast species (known as "Crabtree positive" or C+), there is a critical dilution rate value, D_c, beyond which one observes a striking yield coefficient decrease and a biomass drop is also observed. For this same value D_c, the specific oxygen consumption rate reaches a plateau and the metabolism goes from a respiratory to a respirofermentative mode. At the same time, fermentation products, like ethanol, appear in the medium. As an example, profile of biomass versus dilution rate exhibits a sharp discontinuity in $D = D_c$. This discontinuity is particularly well marked and accurate and, according to our experience, it is impossible to work exactly at this critical value. The threshold value thus looks like a point of discontinuity, in the mathematical sense of the term. It is the same with the specific oxygen consumption rate, specific fermentation products secretion rate, etc. All these phenomena indicate that there is a critical dilution rate value for which the C+ yeasts exhibit an abrupt switch in metabolic pathways, from respiratory to respirofermentative metabolism, when the hydraulic constraint of the system (the dilution rate) exceeds a particular value.

The Crabtree effect has been known for a long time (Crabtree, 1929) and in spite of many studies (De Deken, 1966; von Meyenburg, 1969; Barford and Hall, 1979; Barford et al., 1981; Rieger et al., 1983; Sonnleitner and Käpelli, 1986; Postma et al., 1989; Van Urk et al., 1989; Wojtczak, 1996; Cortassa and Aon, 1998; Bellgardt, 2000a), it has not received up to now a clear and univocal explanation (Walker, 1998; Bellgardt, 2000a). The interpretation of the phenomenon is however of first importance, in particular from an industrial point of view. Indeed, the "levurists", which only have the role of producing biomass, try to avoid fermentation by-products, even thought fermentation industries may find it beneficial to produce these by-products in optimal quantities and thus to decrease the biomass production to the maximum. In addition, some cancerous cells cultures also show a Crabtree effect (for Refs., see Wojtczak, 1996) and the elucidation of this one could have important consequences in the medical field.

We do not claim to bring a final response to the problem, but we only try to contribute to the elucidation of the phenomenon by means of new modeling concepts. We deal with bioreactors representation as polyphasic dispersed systems (PDS; Thierie, 1997). In a PDS representation, all the phases of the system (solid, liquid and gas) are taken into account. The interfaces are disrupted and all the phases are intimately "mixed": we say that the phases are dispersed. The mass balances must thus be calculated for each phase and for each compartment that possibly constitutes one or more phase. The partition in several phases introduces particular interphasic exchanges flux, which do not usually appear in other models. It results in a finer level of description of the phenomenon, which is between the global system (the bioreactor, for example) and the cell. At the cellular phase level, transport and metabolization (T/M) terms are used to represent the metabolization phenomena, the secretion phenomena, etc. Our previous work (Thierie, 1997, 2000) used these terms in an implicit form, i.e. without representing the explicit transport and/or metabolization kinetics. For this study, we derived a very simplified explicit form of the T/M pathways. This simple form allows taking the main phenomena of long-term Crabtree effect into account and this in a very convincing way. The method has been applied to *Saccharomyces cerevisiae* cultivated in aerobic chemostat with glucose as limiting substrate and in a homofermentative case of ethanol production. The model shows that the sharp transition can be explained by a simple kinetic mechanism. However the method goes further, for it gives the possibility to calculate some "general" metabolic flux (specific rates, in fact) and to assess the stoichiometric coefficients of the general equation for glucose metabolization and fermentation in *S. cerevisiae* under aerobic conditions.

At first, we present the model in a very general way; we apply then this model to the Crabtree effect. In a third part, which can be also regarded as a confirmation of the coherence of the PDS approach, we obtain the main metabolic specific rates and the stoichiometric coefficients of the general molar an elementary equation.

2. Methods

When a biological system is represented as a polyphasic dispersed system (PDS; i.e. formed of several phases separated by disrupted interfaces), new interphasic transfer flux is necessary highlighted that are absent from other modes of representation. For each phase, it is necessary to obtain a mass balance that takes into account some exchange flux as well as various transport and transformation kinetics (Thierie, 1997). It is enough for the needs of this work to consider a biphasic "chemostat", made up of a cellular phase (of

superscript c) and of a dispersing matric phase (of superscript m). The working conditions applied to the chemostat were already described previously (Thierie, 2000).

In a chemostat, the substrate mass balance in the cellular phase is

$$\frac{\mathrm{d}\tilde{C}_S^c}{\mathrm{d}t} = -D\tilde{C}_S^c + \Phi_{S,m}^0(c) - q_S^c(.)X^c + \tilde{C}_S^c \frac{\mathrm{d}\ln N_T^c}{\mathrm{d}t}, \quad (2.1)$$

where D is the dilution rate; $\tilde{C}_S^c$, the pseudo-homogeneous concentration (or E-concentration) of substrate S in the cellular phase; $\Phi_{S,m}^0(c)$, the total interphasic exchange flux (in the direction mc) per volume unit; $q_S^c(.)$ is the specific transport/metabolization (T/M) rate of substrate in the cellular phase. X^c is the biomass and N_T^c is the total number of cells.

In the matric phase, the substrate mass balance is

$$\frac{\mathrm{d}\tilde{C}_S^m}{\mathrm{d}t} = D(\tilde{C}_S^{m,E} - \tilde{C}_S^m) - \Phi_{S,m}^0(c), \quad (2.2)$$

where $\tilde{C}_S^{m,E}$ and $\tilde{C}_S^m$ are substrate concentrations in the matric phase, respectively in the feed and in the bulk of the bioreactor.

Steady states of (2.1) and (2.2) are respectively

$$\Phi_{S,m}^0(c) = q_S^c(.)X^c + D\tilde{C}_S^c \quad (2.3)$$

and

$$\Phi_{S,m}^0(c) = D(\tilde{C}_S^{m,E} - \tilde{C}_S^m). \quad (2.4)$$

By dividing this last expression by the biomass, one finds an expression for the specific interphasic transport rate (a specific rate being a flux per biomass unit)

$$\frac{\Phi_{S,m}^0(c)}{X^c} = \frac{D}{Y_{X^c,S}}, \quad (2.5)$$

where $Y_{X^c,S}$ is the substrate-related yield coefficient:

$$Y_{X^c,S} = \frac{X^c}{(\tilde{C}_S^{m,E} - \tilde{C}_S^m)}. \quad (2.6)$$

Relations (2.1)–(2.4) constitute the implicit form of the PDS representation because the net specific rate $q_S^c(.)$ is not expressed according to state variables and parameters. This specific rate is normally expressed in terms of local concentrations, which are relevant in the cellular phase. Thus, if we decide to represent $q_S^c(.)$ by a series of hyperbolic functions

$$q_S^c(.) = \sum_{i=1}^{n} \frac{V_S^0(i)C_S^c}{K_S(i) + C_S^c}, \quad (2.7)$$

where $V_S^0(i)$ is the maximum specific rate of pathway i, $K_S(i)$ the inverse of the "affinity" for the substrate in way i, and C_S^c is the local substrate concentration (or R-concentration), i.e. the intracellular concentration. The intracellular concentrations are, from an experimental point of view, rather difficult to measure and thus to use in a model. Therefore, if account is held that the relation between R and E-concentrations is (Thierie, 1997)

$$C_S^c = \tilde{C}_S^c \frac{\delta_c}{X^c} \quad (2.8)$$

the local kinetics can be expressed in terms of global state variables. δ_c is the volumetric mass of the cellular phase (in g/l, for example).

The explicit model that we use to represent the Crabtree effect at steady state in *S. cerevisiae* are based on the following criteria:

- The explicit form of the specific transport/metabolization rate has the same form as Eq. (2.7) with $n = 2$.
- Relation (2.8) applies.
- There are two T/M pathways ($n = 2$), one with low maximum specific rate (lower than the washout) and with high affinity for the substrate; the other, with very low affinity for the substrate, corresponding to a first-order reaction in relation to S.

Under these conditions, the net T/M specific rate becomes

$$q_S^c(.) = q_S^c(h) + q_S^c(l) = \frac{V_S^0\tilde{C}_S^c}{K_S^*X^c + \tilde{C}_S^c} + \tilde{C}_S^c k_0^*/X^c \quad (2.9)$$

with

$$K_S^* = K_S(1)/\delta_c, \quad (2.10)$$

$$k_0^* = k_0\delta_c = (V_S^0(2)/K_S(2))\delta_c \quad (2.11)$$

and

$$q_S^c(h) = \frac{V_S^0\tilde{C}_S^c}{K_S^*X^c + \tilde{C}_S^c}, \quad K_S^* \ll 1, \quad (2.12)$$

$$q_S^c(l) = k_0^* \frac{\tilde{C}_S^c}{X^c}. \quad (2.13)$$

Using Eq. (2.9) in the expression of the steady state (2.3), it can be shown that the mass balance takes the form of a second degree polynomial in $\tilde{C}_S^c$ with variable coefficients:

$$P^2(\tilde{C}_S^c) \equiv a_2'(\tilde{C}_S^c)^2 + a_1'\tilde{C}_S^c + a_0' = 0 \quad (2.14)$$

with ($\Phi_S^0 \equiv \Phi_{S,m}^0(c)$)

$$a_0' = -K_S^*X^c\Phi_S^0,$$

$$a_1' = X^c(V_S^0 + K_S^*(D + k_0^*)) - \Phi_S^0, \quad (2.15)$$

$$a_2' = D + k_0^*,$$

which admits a single nonnegative real solution:

$$\tilde{C}_S^c = \frac{-a_1' + \sqrt{(a_1')^2 - 4a_2'a_0'}}{2a_2'}. \quad (2.16)$$

When the affinity of the high-affinity pathway 1 tends towards infinity ($K_S^* = 0$), relation (2.16) tend towards

the function

$$\tilde{C}_S^c = \frac{-a_1' + |a_1'|}{2a_2'}. \tag{2.17}$$

This function vanishes when a_1' is positive and takes a finite positive value when a_1' is negative. It thus presents a sudden transition from a zero to a positive value for $a_1' = 0$. It is easy to show that the critical dilution rate (or threshold) is given by

$$D_c \approx V_S^0 Y_M \tag{2.18}$$

provided that K_S^* is small enough. (The meaning of Y_M will be given later). Relation (2.18) is fundamental for the comprehension of phenomena appearing in Crabtree-positive yeasts. At first, the Crabtree effect will only appear if the dilution rate is lower than the washout rate ($D_c < D_W$); then, with constant Y_M, one notes that the emergence of the transition entirely depends on the high-affinity T/M rate. This result confirms those obtained by Van Urk et al. (1989). From our point of view, independent of the mechanisms involved in transport processes, the Crabtree-positive yeasts are those for which the maximum specific rate of the high-affinity pathway (V_S^0) satisfies $D_c < D_W$; the Crabtree-negative yeasts exhibit a sufficiently high V_S^0 and so $D_c > D_W$ (roughly speaking, Crabtree-negative yeasts are characterized by $V_S^0 > \mu_{\max}/Y_M$).

Let us rewrite the implicit balance (2.3) by taking account of (2.9):

$$\Phi_S^0 - (q_S^c(h) + q_S^c(l))X^c - D\tilde{C}_S^c = 0 \tag{2.19}$$

and let us imagine that part of the substrate leaves the cellular phase in the form of metabolites $\{P_i\}$. Let us define

$$\beta q_S^c(l) X^c \quad \text{the fraction which remains in the cellular phase,} \tag{2.20}$$

$$(1-\beta) q_S^c(l) X^c \quad \text{the fraction which leaves this one.} \tag{2.21}$$

After excretion, the substrate balance in the cellular phase becomes

$$\Phi_S^0 - (q_S^c(h) + \beta q_S^c(l))X^c - D\tilde{C}_S^c = 0. \tag{2.22}$$

It is obvious that the two balances (2.19) and (2.22) cannot simultaneously be satisfied. The solution consists in modifying the biomass in Eq. (2.19) so as to satisfy the two balances. We easily obtain from Eq. (2.19) that the new biomass value is given by

$$X^{/c} = \frac{\Phi_S^0 - D\tilde{C}_S^c}{q_S^c(h) + q_S^c(l)}. \tag{2.23}$$

We have shown that $X^{/c} \leqslant X^c$. Biomass decrease is thus the result of the mass balance reinstatement.

Now, let us describe the algorithm used to calculate this biomass drop.

Solution of Eq. (2.14) requires knowing the state variables X^c and S. These last ones can be produced by an auxiliary "model" we call the generator model or can be obtained in experiments. The generator model that we previously used was the Monod's model. (The value of Y_M appearing in Eq. (2.18) is "the yield coefficient" of the Monod's model. It does not generally represent the true yield coefficient of the system, which is not constant for all D).

The straightforward algorithm does not require any conditional test nor any optimization condition and is as follows:

Beginning ($D = 0$)

a. calculate $S(D)$ via a generator model or use a fitting of experimental data,

b. calculate $X^c = Y_M(S^0 - S)$,

c. calculate $\tilde{C}_S^c$ via (2.16),

d. calculate q_S^c via (2.9),

e. calculate $X^{/c}$ via (2.23),

f. increment D and go back to a. (2.24)

End ($D = D_w$)

Note that the calculation of X^c at step (b) is always possible, even without using a generator model. Y_M then becomes a simple constant without particular meaning (even if it keeps "the form" of a yield coefficient).

We must now calculate the metabolites excreted related to the respirofermentative pathway (like ethanol (EtOH) or CO_2). One of the advantages of our method is its capacity to permit the calculation of specific rates in an isolated reaction pathway even if all the biochemical details are not known. For example, at the start of a substrate, we can avoid representing the intermediate steps that lead to end products $\{P_i\}$. However, all expressions used up to now are expressed in equivalent-substrate and we must find (for example) the metabolites concentrations (EtOH, CO_2, ...). To do so, we use a mass ratio coefficient (MRC), which can be defined as follows.

Let consider a single reaction pathway within the cellular phase:

$$v_S S \to \cdots \to v_1 P_1 + v_2 P_2 + \cdots v_i P_i + \cdots \tag{2.25}$$

where v_k are stoichiometric coefficients (negative on the left- and positive on the right-hand side). $\{P_i\}$ are end products of the transformation.

We call mass ratio coefficient the positive definite quantity

$$\rho_{Pi,S} = \left| \frac{v_{Pi} MM_{Pi}}{v_S MM_S} \right|, \tag{2.26}$$

where MM_k is the molar mass of k.

One can show that

$$\tilde{C}_{Pi}^x = \rho_{Pi,S} \tilde{C}_S^x, \quad x = c, m, \ldots \tag{2.27}$$

and that

$$q^c_{Pi} = \rho_{Pi,S} q^c_S. \tag{2.28}$$

Although the reasoning is not exactly rigorous, we can calculate the metabolite concentration in the matric phase in the following way.

Taking Eq. (2.21) into account, the mass balance of the substrate excreted in the matric phase can be put in the form (in equivalent-substrate):

$$\frac{\mathrm{d}\tilde{C}^m_S}{\mathrm{d}t} = (1-\beta) q^c_S(l) X^{/c} - D\tilde{C}^m_S \tag{2.29}$$

for which the steady state is

$$\tilde{C}^m_S = (1-\beta) q^c_S(l) X^{/c}/D. \tag{2.30}$$

Multiplying the left- and the right-hand side by (2.26) and using (2.27), it turns out that

$$C^m_{Pi} = \rho_{Pi,S}(1-\beta) q^c_S(l) X^{/c}/D \tag{2.31}$$

which expresses the metabolite concentration P_i in the matric phase. The general implicit form of (2.31) is

$$C^m_{Pi} = \rho_{Pi,S} q^c_S(*) X^{/c}/D, \tag{2.32}$$

where $q^c_S(*)$ represents the fraction of the specific excretion rate expressed in equivalent-substrate. Algorithm (2.24) and relation (2.31) are sufficient to calculate the biomass drop and the metabolites concentrations associated with the excretion of the substrate.

To summarize, when metabolite excretion is considered, our approach makes it possible to model the decoupling between substrate consumption devoted to growth and fraction used to something else, like excretion of fermentation products. This last approach is particularly fruitful, since it leads to the possibility of visualizing the distribution of the principal specific rates (or principal flux) of the substrate metabolism. Scheme 1 shows a manner of representing this distribution in the cellular phase (showed like a simple cell).

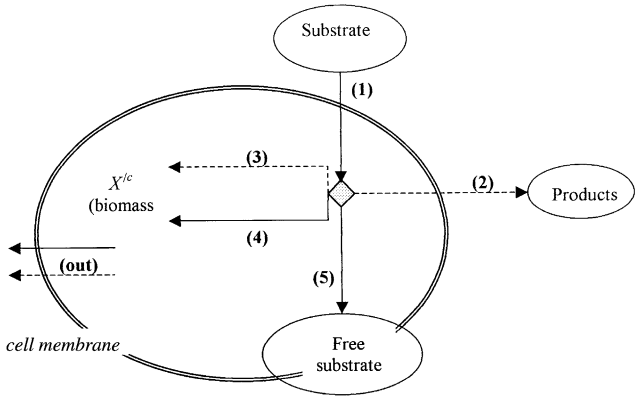

Scheme 1. Main specific rates distribution in cellular phase (presented here has an "isolated cell"). (1) Total T/M specific rate: $q^c_S = q^c_S(h) + q^c_S(l)$; (2) excretion $(1-\beta)q^c_S(l)$: anabolism/fueling; (3) $\beta q^c_S(l)$ and (4) $q^c_S(h)$; (5) Free substrate: $D\tilde{C}^c_S/X^{/c}$; (out) output term taking the yield coefficient (not quantified) into account. Dashed lines only show metabolic pathways activated for $D > D_c$.

The arrow (1) indicates the total substrate T/M flux. The high-affinity pathway (4) is permanent and feeds anabolism and fueling pathways (with an output way (**out**), not quantified here, for water, CO_2,…). The arrows (2) and (3) represent the low-affinity pathway, which is only triggered beyond the critical point (an exit point (**out**) is also associated with this mechanism). The arrow (5) represents the free substrate, adsorbed on the membrane and/or present in the cell. In this representation, there is "a nodal point" which represents the connection of the principal pathways of anabolism/fueling, of excretion and of free substrate. The dashed lines indicate the pathways which are activated for $D > D_c$. The way (5) may also vanish below the critical point or become negligible on the whole dilution rates interval (this last situation depending on the value of k_0^*). All in all, for $D < D_c$, only the ways (1) and (4) are active; all the substrates are used for biosynthesis and fueling reactions. For $D > D_c$, pathway (4) saturates and reaches its maximum value. Pathways (2), (3) and (5) are activated. Biosynthesis is then ensured via pathways (3) and (4). Pathway (2) is used for substrate transformation and formation of products excreted in the matric phase.

3. Results

3.1. Opening remarks

3.1.1. Experimental data

Since the original article (Crabtree, 1929), many authors described the Crabtree effect in yeasts. We chose the experimental data of Rieger et al. (1983), in *S. cerevisiae*, mainly because they are made of three series of measurements carried out under same experimental conditions, except for the glucose concentration in the feed of the chemostat ($S^0 = 5$, 10 and 30 g/l). These data allow comparison with the model in three different situations, each relating to the same real system. (We will not study here the data concerning cultivation on glucose/ethanol mixtures presented by the same authors. These experiments, manageable by our model, are left for a later publication.)

In spite of these advantages, experimental data of Rieger et al. present some drawbacks. It is at first necessary to distinguish the "true" experimental data (which are measured) from calculated or estimated data. The first category belongs to the external "data": dilution rate and glucose feed concentration; no error measurement is associated with these two values. If we can generally admit that the concentration in the feed is very precise (negligible error), it is not the same for dilution rate that is usually biased with a significant error. The three other measured quantities (biomass, substrate and ethanol) are the average values of at least

three measures and the standard deviation is given. These measurements present in general very high dispersion, mainly for glucose measurement (of which relative errors vary between 25 and 48%). This situation is particularly unfavorable for parametric estimation (see following section). The precise measurement of residual substrate is usually known to be rather problematic (Roels, 1983). In some cases, the dispersion of the results concerning biomass (in dry weight) is also very high; for instance, for $S^0 = 30$ g/l, the relative error on the biomass vary from only 1% to up to 30%.

Moreover, the two other sets of "experimental data" (specific oxygen uptake rate and specific carbon dioxide production rate) are not directly measured values, but calculated by approximations partially based on the fact that only CO_2 and ethanol (EtOH) are produced during fermentation. Verification of the homofermentative character of the culture is carried out by the authors on the basis of carbon balance. Although these quantities are calculated values, we will use them, within the framework of this study, like experimental values.

Another cumbersome pitfall for our work relates to the biomass measurement procedure. Harvested broth has been centrifuged, washed and dried until constant weight. This method is perfectly valid, but the washing operation probably eliminates the glucose adsorbed on the cells. The quantity of adsorbed glucose would have been invaluable for the assessment of the model, which integrates this data in the mass balances. In addition to this, incautiously drying eliminates the volatile products and does not allow determining the EtOH content in the cellular phase. However, in probable absence of significant ethanol accumulation (Guijarro and Lagunas, 1984; D'Amore et al. 1988), we have shown that this loss of information is insignificant.

3.1.2. Parametric estimation

Although the number of parameters to be estimated is low (only 5), the general estimation procedure is delicate. The simplest cases (estimation of one or several parameters using two state variables $\{\lambda(i)\} = f(X, Y)$), can be easily solved using simple software package. However, other situations need a parametric estimation requiring more than two state variables $\{\lambda(i)\} = f(X, Y, \ldots, Z)$). In these more complex cases, we have used a visual fitting procedure, associated with a least-squares calculation. This method provides relatively rough results and certainly deserves the development of a more advanced protocol. Nevertheless, the obtained results are sufficient to assess adequacy between simulations and experimental data, even if precision and statistics on parametric estimation can be improved.

It would be too long to explain precisely how the value of each parameter could be obtained, but general guidelines are the following ones:

- A pre-estimation of Y_M is carried out by simple arithmetic mean of the experimental data at low dilution rates ($D < D_c$). This parameter is a constant in the generator model and only occasionally corresponds to the yield coefficient of the system.
- The value of D_c is roughly estimated by a graphic method on the curve $X^c(D)$;
- A pre-estimation of V^0_{GLU} is obtained via $V^0_S \approx Y_M/D_c$ (cf. (2.18));
- Using these pre-estimations as initial guesses, the theoretical curves are fitted through biomass, ethanol and specific interphasic exchange rate (*SIER*) data. The five parameters are manually adjusted on the basis of a least-squares calculation (sum of least squares on the three curves).

The results are included in Table 1.

The values of Table 1 will be used for all simulations.

Comments.

(a) Results of the parametric estimation indicate that the values obtained are true constants, independent both of glucose concentration in the feed and of dilution rate.

(b) The value estimated for K^*_{GLU} strongly depends on the more or less acute shape of the transition around the threshold ($D = D_c$). We only had one experimental point close to this zone, which leaves a great uncertainty on this parameter. It can be considered that it is only estimated at one order of magnitude (between 1×10^{-5} and 1×10^{-7}; $\mathrm{p}K^*_{GLU} = 6 \pm 1$). For general representation of the phenomenon, the curves are not very sensitive compared to K^*_{GLU}, except precisely in a narrow neighborhood around transition. In literature, the value of the transport half-saturation constant (affinity) is about $K_m = 1$ mM (Walsh et al., 1994), which corresponds to approximately 0.18 g GLU/l.

We find a value of K_{GLU} ranging from 10^{-2} to 10^{-4}, which, for a biomass of 10 g/l, corresponds to an affinity included in the interval of 10^{-1} and 10^{-3} g/l. Although the lower limit of this interval is compatible with K_m, it is clear that the central value (average) is much lower than the transport affinity estimation. In fact, the two

Table 1
Results of parametric estimation

S^0 (g/l)	5	10	30	g/l
Y_M	0.480	0.474	0.474	g/g
K^*_{GLU}	1×10^{-6}	1×10^{-6}	1×10^{-6}	—
V^0_S	0.61	0.62	0.62	h^{-1}
k^*_0	25	25	25	h^{-1}
β	0.100	0.105	0.105	—
K_{GLU}[a]	1×10^{-3}	1×10^{-3}	1×10^{-3}	g/l
k_0[a]	2.5×10^{-2}	2.5×10^{-2}	2.5×10^{-2}	l/(g h)

[a] Values calculated on the basis of a biomass volumetric mass of 1000 g/l, by using relations (2.10) and (2.11).

parameters don't have the same meaning. K_m value is measured under experimental conditions such as the only transport is taken into account (very fast measurements, work at low temperature, etc), even though K_{GLU} measures an affinity resulting from transport and metabolization in the steady state. The same remark evidently applies for the maximum transport rate $V_{\max}$ and for the T/M rate, V_S^0.

(c) The $\{k_0^*, \beta\}$ couple is very interdependent, especially for low values of k_0^*. The precise value of this parameter can only be found if the "free" glucose (adsorbed or other) in the cellular phase is known. As we specified, these experimental data are not available and we have chosen a reasonable value by estimating that free glucose in the cellular phase was low (a few percents of the concentration in the feed; Walsh et al., 1994).

(d) The Y_M value used in algorithm (2.24), is a constant on the whole interval of D. It numerically coincides with the yield coefficient only for dilution rates lower than the threshold. The true yield coefficient $Y_{X/c,GLU}$ is obviously variable with D beyond the threshold value.

3.2. Model assessment

3.2.1. Residual substrate representation

Algorithm (2.24) requires the calculation of the substrate on the whole dilution rates interval under study. This is necessary to calculate the other state variables in intermediary points between those of the experiment. With this intention, we used two different methods:

(i) The first, known as experimental (EXP), consists in using an interpolation function for the experimental data. This interpolation function (fitting) does not make physical sense but must present a correlation coefficient as high as possible. Its applicability is theoretically valid from the first to the last experimental value. We have however used this function on a slightly wider interval. For these additional values, it can be expected (in the absence of discontinuity) that the variations between the calculated values and the real values are smaller than the average experimental error (rather high, let us point out it). As an example, Table 2 shows the functions that we used to calculate the residual substrate on the interval $D \in [0.20, 0.41]$.

(ii) The second method makes use of a generator model (GM) of Monod type. In the steady state, the residual substrate in the Monod's model is

$$S = \frac{D.K_M}{\mu_{\max} - D} \tag{3.1}$$

where $\mu_{\max}$ is the maximum specific growth rate and K_M the half-saturation constant. With the data of Rieger et al. (1983), simultaneous estimation of these two parameters is delicate and the convergence of some methods is not ensured. We thus proceeded in two stages. At first, an estimation of (3.1) has been carried out without constraint. The results appear in Table 3.

It is clear that $\mu_{\max}$ is a constant whereas K_M is a function of the feed concentration. The uncertainty on K_M is high and low for $\mu_{\max}$. We have then fixed this value at an average value of 0.44 and readjusted (3.1) using this value as a constraint. The new values of K_M are included in Table 4.

These last values of K_M are more precise and were used for simulations.

Note: K_M still changes according to feed concentration in a roughly linear way (data not shown). This clearly states that, contrary to the maximum growth rate, the "affinity" for the substrate is not a constant. The culture is not well represented by the Monod's

Table 3
Fitting of Eq. (3.1) without constraint

S^0 (g/l)	$\mu_{\max}$ (h^{-1})	K_M (g/l)	r^2
5	0.44 ± 0.01	0.23 ± 0.08	0.95
10	0.45 ± 0.02	0.36 ± 0.16	0.91
30	0.43 ± 0.01	0.41 ± 0.15	0.96

Table 2
Residual substrate fitting (EXP)

S^0 (g/l)	Function	Parameters	r^2
5	$\exp\left(a + b\frac{\ln D}{D^2}\right)$	$a = 4.217129316$ $b = 0.403164303$	1.000
10	$\exp\left(a + b\frac{\ln D}{D^2}\right)$	$a = 2.266763740$ $b = 0.297104130$	0.994
30	$a\exp\left(\frac{t1 + t2}{t2}\right)^{t2}$, $t1 = (D-b)/c$, $t2 = d-1$	$a = 6.721420183$ $b = 0.574567450$ $c = 0.147947931$ $d = 2.982587130$	1.000

model, where K_M is a true constant. This confirms that the affinity for the substrate is not a constant. However, it depends on biomass and not on feed concentration (although the biomass change with S^0).

3.2.2. Biomass representation

Once S and Y_M are fixed, the representation of the biomasses of the generator model, X^c, and of the true system, $X^{/c}$, are easily calculated as described in the algorithm (2.24).

3.2.3. Ethanol representation

Next step in parametric estimation necessitates representing the EtOH concentration. Our method allows calculating a specific rate without necessarily knowing the details of the metabolic reactions (because specific rates are conservative, it is only necessary to know the first and the final compounds in a reaction chain to obtain the relation between the respective rates. Details about how the final product is formed are not required). We simply admit that the ethanol production takes place via the following total reaction:

$$GLU \rightarrow 2EtOH + 2CO_2(f) \tag{3.2}$$

where GLU is glucose. The symbol f indicates that CO_2 is produced by fermentation. By using the mass coefficient ratio (2.26), we express the relation between the specific EtOH rate and that expressed in substrate-equivalent (cf. (2.28)):

$$q^c_{EtOH} = \rho_{EtOH,GLU} q^c_{GLU}(*) \tag{3.3}$$

The following relation expresses the explicit EtOH excreted fraction (cf. (2.21)):

$$q^c_{EtOH} = \rho_{ETOH,GLU}(1-\beta) q^c_{GLU}(l). \tag{3.4}$$

The ethanol concentration in the matric phase is then (cf. (2.32))

$$\tilde{C}^m_{EtOH} = \frac{q^c_{EtOH} X^{/c}}{D}. \tag{3.5}$$

The same reasoning applies to the CO_2 of the fermentative pathway and

$$q^c_{CO_2(f)} = \rho_{CO_2(f),GLU}(1-\beta) q^c_{GLU}(l), \tag{3.6}$$

$$\tilde{C}^m_{CO_2(f)} = \frac{q^c_{CO_2(f)} X^{/c}}{D}. \tag{3.7}$$

This last pseudo-homogeneous concentration represents the CO_2 dissolved in the matric phase, without additional degasification nor (bio)chemical reactions. (It is undoubtedly not a directly measurable quantity over a wide pH range.) The mass coefficient ratios are calculated by using Scheme (3.2) and relation (2.26):

$$\rho_{EtOH,GLU} = 0.511 \tag{3.8.a}$$

and

$$\rho_{CO_2,GLU} = 0.489. \tag{3.8.b}$$

3.2.4. Specific interphasic exchange rate (SIER)

An important quantity for the parametric estimation is the specific interphasic exchange rate defined by

$$SIER = \frac{\Phi^0_{GLU}}{X^{/c}} \tag{3.9}$$

which is easily computable using experimental data.

Figs. 1–3 show the biomass, ethanol and substrate profiles for the three feed concentrations. (Parameters of

Table 4
Fitting of Eq. (3.1) with $\mu_{max} = 0.44$

S^0 (g/l)	K_M (g/l)	r^2
5	0.222 ± 0.018	0.95
10	0.302 ± 0.033	0.92
30	0.568 ± 0.048	0.96

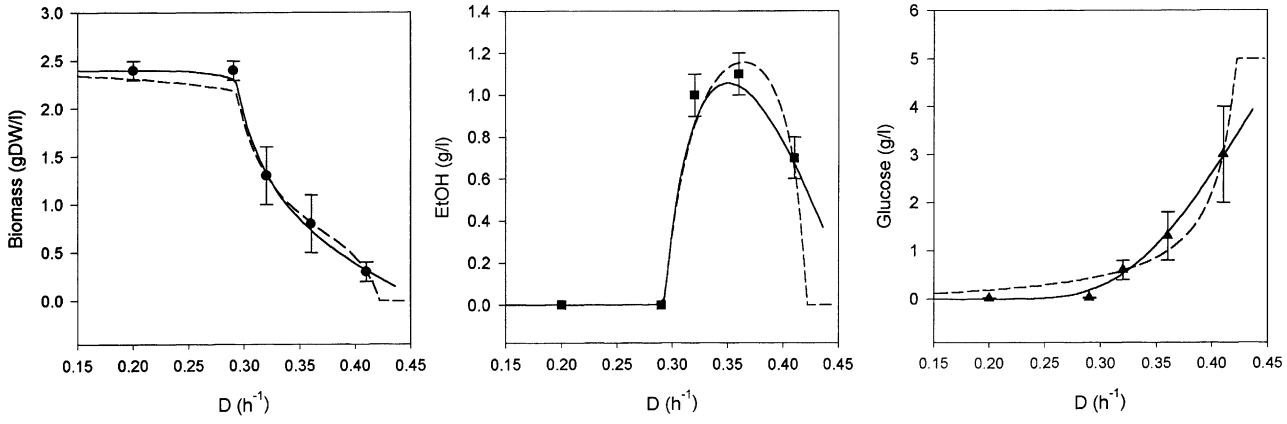

Fig. 1. Main state variables profiles for $S^0 = 5$ g/l. *Method*: Simulations were carried out by using the algorithm (2.24) and parameters listed in Table 1. Full lines represent simulations obtained by the EXP method; dashed lines were obtained by the generator model (GM) method (Monod). *Comments*: One notes a significant difference between substrate profiles according to the method used for residual substrate computation (EXP or GM). Ethanol profile is more sensitive to the way in which the substrate is represented (EXP or GM) than the one of biomass.

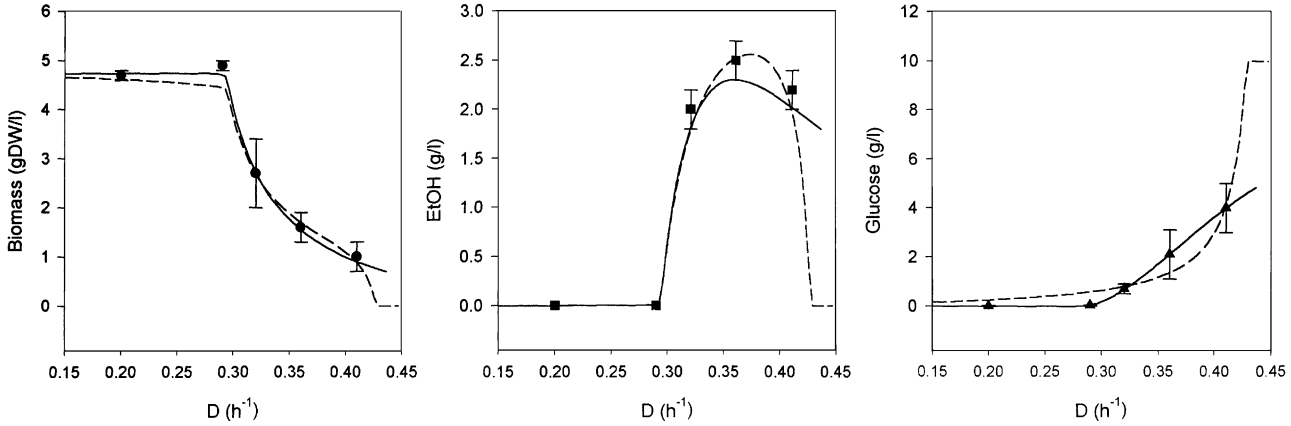

Fig. 2. Main state variables profiles for $S^0 = 10$ g/l. *Method and comments*: as in Fig. 1.

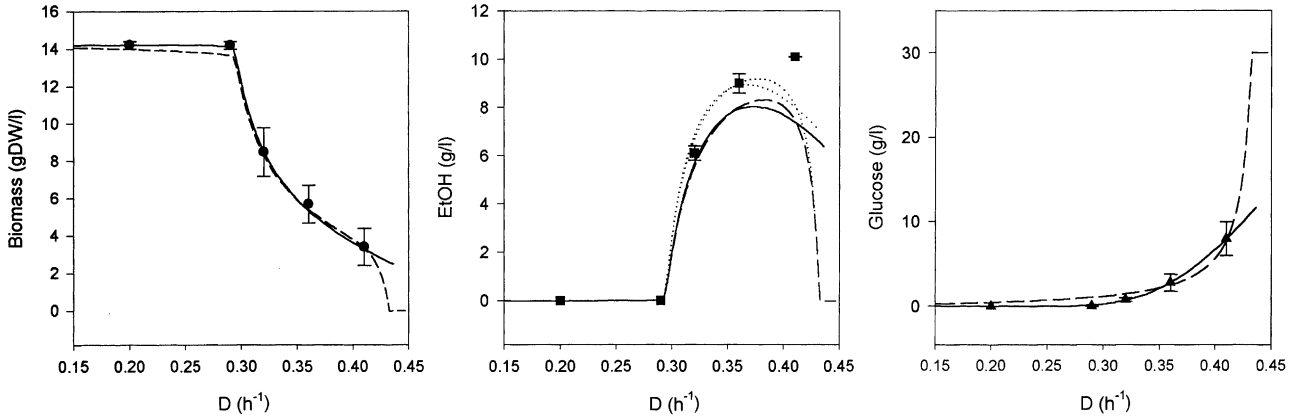

Fig. 3. Main state variables profiles for $S^0 = 30$ g/l. *Method*: as in Fig. 1. *Comments*: one notes a better convergence between EXP and GM methods for the representation of the residual substrate. As a consequence, biomass and ethanol exhibit very close profiles. One notes however a worse agreement between some ethanol experimental data and simulations. The dotted lines represent simulations with $\beta = 0.075$. Even with this correction, the last experimental point remains significantly far from the calculated profiles. We think that this experimental value, because of its singularity, may be doubtful (for a discussion, see text).

Table 1 were used for simulations.) Full line curves were obtained for substrate representation by "experimental" fitting (EXP), dashed line curves, by using the generator model (GM).

Fig. 4 shows the specific interphasic exchange rate (3.9) and Fig. 5, the true yield coefficient (2.6). It is noticed that these two series of curves are invariants compared to the substrate feed concentration.

Generally speaking, agreement between simulations and experimental data are very good. However it is noted that profiles significantly vary according to the mode of representation of the substrate we used (EXP or GM). Roughly speaking, the profile in biomass is always better in EXP representation; it is (obviously) the same for the substrate. This fact, combined with the dependence of K_M according to S^0, encourages us to think that the GM is a worse representation and that the system deviates from the Monod's model, contrary to what certain authors claimed (Sonnleitner and Käpelli, 1986).

Note: The EtOH (D) curve for $S^0 = 30$ g/l is of poorer quality than for the other feed concentrations, especially for $D > 0.35\,\mathrm{h}^{-1}$. The result can be largely improved by introducing a corrective term into (3.4):

$$q^c_{EtOH} = \varepsilon \rho_{EtOH,GLU}(1-\beta) q^c_{GLU}(l). \tag{3.10}$$

The ε value is about 1.03 and the correction is small. However, this correction procedure is not very satisfactory for it disturbs the balance between what is excreted and what remains in the cellular phase. Another way consists in fitting the curve by using only the EtOH profile (and not the other ones, like biomass, *SIER*, etc.). One then obtains a value of β close to 0.075 (dotted curve on Fig. 3). In spite of this new value, the adjustment is not perfect. Moreover, the other profiles (particularly concerning biomass) are definitely poorer. We must thus consider that the values tabulated in Table 1 remains the best compromise to account for the whole of the curves obtained in experiments (and thus that β is a constant for all the feed concentrations). Let

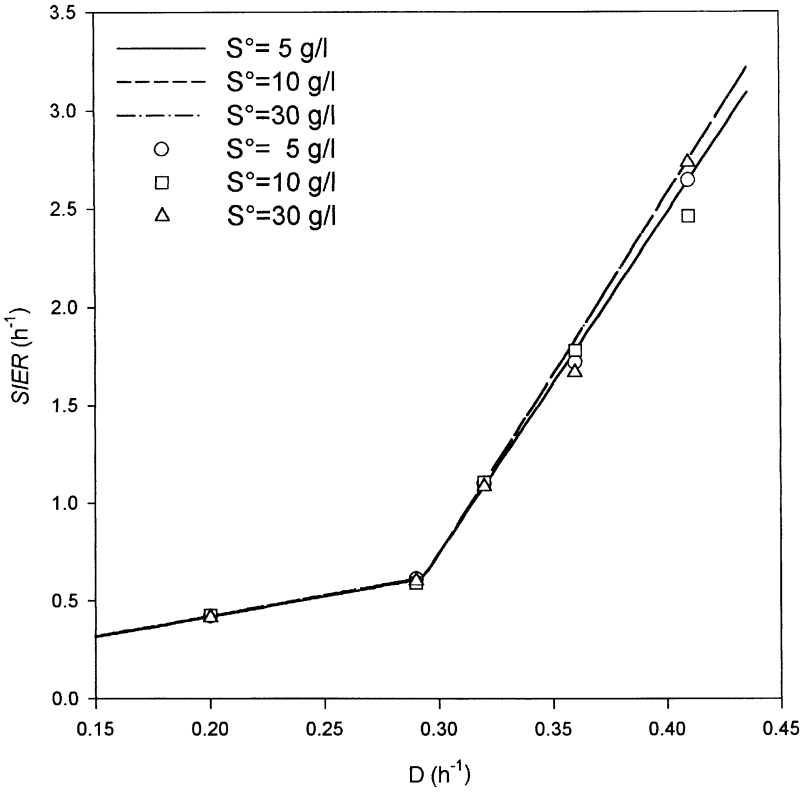

Fig. 4. Specific interphasic exchange rate profile for the three feed concentrations. *Method*: Simulations have been carried out by using the algorithm (2.24) and parameters of Table 1, with a representation of the substrate according to the EXP method. *Comments*: Practically, the three curves are confused; the experimental results (averages) dispersion increases with the dilution rate.

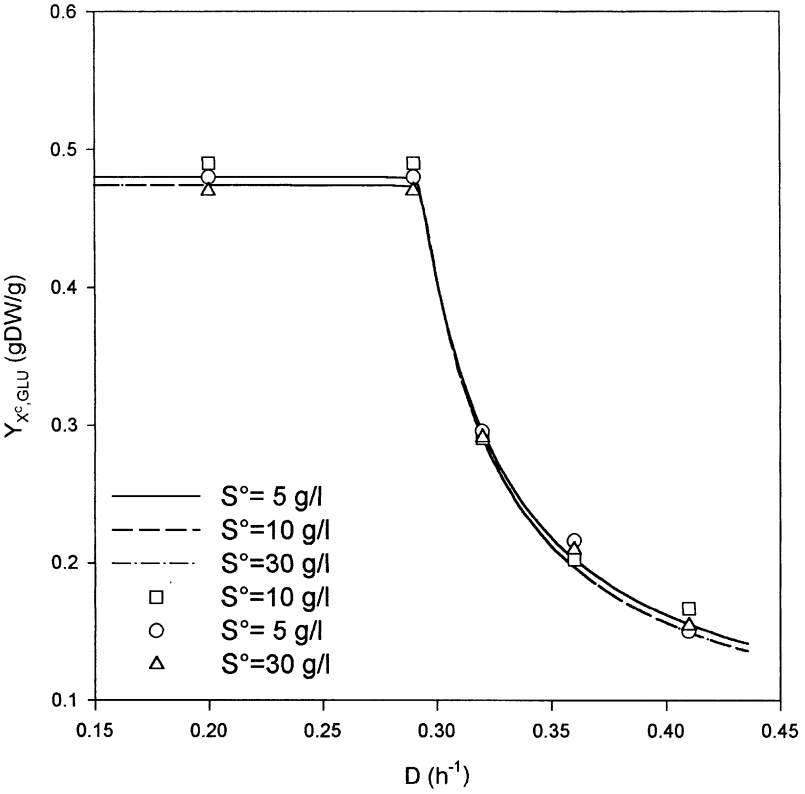

Fig. 5. Yield coefficient profiles for the three feed concentrations. *Method*: as in Fig. 4. *Comments*: The three curves are confused and the dispersion of the results tends to increase with D for $D > D_c$.

us notice that the parameters corrections we talked about are small, ranging from 15% to 25% maximum. Sinceβ is very sensitive to the biomass changes (for which the errors can reach 30%), it is thus not absolutely impossible that fluctuation in the parameter value can be due to the dispersion of measurements in biomass. However, how to explain, in this case, the good agreement of the two other profiles? The most problematic experimental data is the one located around $D = 0.41\,\mathrm{h}^{-1}$. This data is very singular because it reveals a cellular ethanol production almost twofold higher than all the other production values. Moreover, the CO_2 production, which is associated with the production of ethanol, does not present a singularity of this kind (see Fig. 8). In fact, we have good reasons to think that the "problematic" experimental data of Rieger et al. could be either an experimental or a typing one (other errors can be found in the table, in particular concerning some yield coefficients, which are easy to verify). Since each measurement is the average of several rather little dispersed data, the transcription error in the table seems more probable. To sum up, we think that it would be hazardous to build a distinctive corrective hypothesis for one data over 15 that does not coincide with the model. It would be unjustified to build a "theory" about the overproduction of ethanol, occurring near the washout rate and for high glucose concentrations in the feed, just based on a single (perhaps doubtful) value.

3.2.5. Critical dilution rate assessment

We showed (see (2.17)) that the theoretical critical dilution rate (threshold) could be approximated by

$$D_C \approx V^0_{GLU}\, Y_M.$$

Several methods have been used to verify this theoretical value. The results appear in Table 5.

All the values have been obtained in the same way. The experimental data were split in two sets: one for low dilution rates, the others for high ones. Each set was fitted according to a straight line. Finally, intersection of the two lines has provided the threshold value. The method 1 was carried out using the *SIERs*, the method 2 has used the specific total CO_2 production rates and method 3, the specific oxygen uptake rate. Agreement between theory and experiments is excellent (especially for the *SIER*) and provides a value very close to $0.3\,\mathrm{h}^{-1}$.

Table 5
Calculation of D_c

S^0 (g/l)	D_c			
	Theoretical	Method 1	Method 2	Method 3
5	0.293	0.294	0.285	0.307
10	0.294	0.294	0.287	0.308
30	0.294	0.294	0.289	0.294

3.3. Distribution of the specific rates in cellular phase

3.3.1. General presentation

Specific rates calculated up to now are expressed in substrate-equivalent, except for the ethanol and CO_2 produced in the fermentative pathway. We can build the additional specific rates, taking into account that the process is homofermentative. The "lacking" pathways are thus those of biomass, respiratory CO_2 and water production. It is still necessary to add a pathway for hydrogen consumption, required for water formation. The experimental data are insufficient to treat nitrogen and, as in the work of Rierger et al. this element will be absent in the balance.

The specific rates are conservative, i.e. the sum of the partial specific rates is equal to the total specific rate, which is nothing but the specific interphasic exchange rate (*SIER*). Fig. 6 presents the sole logical configuration for the partial specific rates distribution in the cellular phase.

Glucose penetrates in the cellular phase via the way (E). The nodal point (in gray on the diagram) is used as a "turntable" for the fermentative pathway (1), the "way" that preserves some "free" substrate (intracellular or adsorbed on the membrane) (5) and the biosynthesis/fueling pathway, leading to biomass synthesis, water and respiratory CO_2. Hydrogen and oxygen input pathways are necessary to complete the system. The specific rates we have to find out are thus: $q^c_{O_2}$, $q^c_{X/c}$, $q^c_{CO_2(r)}$, $q^c_{H_2O}$ and q^c_H.

3.3.2. Specific oxygen uptake rate

One of the characteristics of the Crabtree effect is to show a typical profile of the specific O_2 rate of the Blackman type (a linear increase followed by a plateau). The specific substrate rate of the high-affinity pathway shows the same profile when K^*_S is sufficiently low. It seemed therefore logical to associate the specific O_2 consumption rate to the high-affinity pathway and to assume a simple relation like

$$q^c_{O_2} = \gamma_{O_2} q^c_{GLU}(h), \tag{3.11}$$

where γ_{O_2} is an empirical dimensionless constant. The values of this constant have been obtained close to the critical dilution rate and are included in Table 6.

The constants present a very weak decreasing trend with the feed concentration (the slope is about -10^{-3}). This variation is low enough to consider the values as independent of S^0. Fig. 7 shows that correspondence between (3.11) and experimental data is good. We can thus reasonably associate the high-affinity pathway of metabolization of glucose with the oxygen uptake.

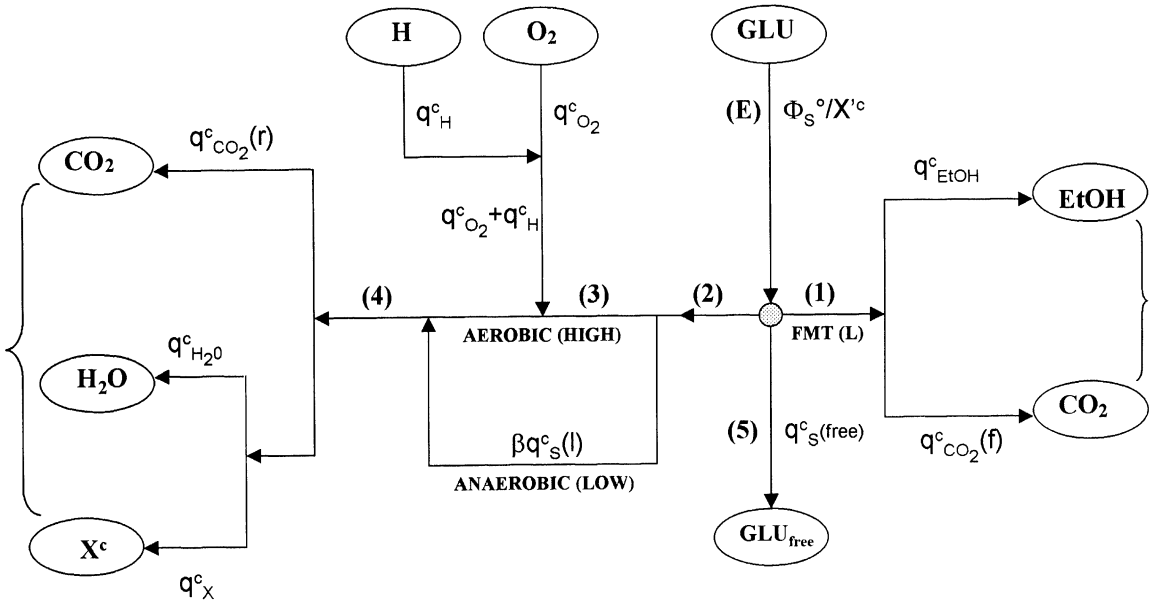

Fig. 6. Distribution of the main specific rates within the cellular phase. (E) Total specific rate of substrate input, $\Phi_S^0/X^{/c}$; (1) the rate of the fermentative (FMT) pathway is a fraction of the low-affinity T/M pathway: $(1-\beta)q_S^c(l)$; (2) specific rate (in substrate-equivalent) of the non-fermentative pathway, including the high-affinity pathway and part of the low-affinity pathway: $q_S^c(h)+\beta q_S^c(l)$; (3) high-affinity specific rate (HIGH, in substrate-equivalent) associated with hydrogen and oxygen uptake constituting the aerobic pathway of glucose metabolization (respiratory pathway); (4) sum of metabolization rates contributing to biosynthesis and associated fueling: $q_S^c(h)+\beta q_S^c(l)+q_{O2}^c+q_H^c$; (5) rate associated to the "free" substrate (adsorbed and/or intracellular). The gray point on the figure is called "nodal point" and constitutes a "turntable" for the distribution of the specific rates (expressed in substrate-equivalent).

Table 6
Values of γ_{O_2}

S^0 (g/l)	γ_{O_2}
5	0.441
10	0.421
30	0.418

Note: A specific rate decrease seems to occur for $D > 0.4\,h^{-1}$. A similar but more marked phenomenon has already been observed (von Meyenburg, 1969) and has been interpreted like an artifact (Nielsen and Villadsen, 1994). Other studies show a better plateau (Barford and Hall, 1979; Barford et al., 1981). The Blackman profile for q_{O_2} is now widely accepted.

3.3.3. Specific biomass production rate (or specific growth rate)

According to our working conditions of the chemostat, it results that biomass specific production is

$$q_{X/c}^c = D \tag{3.12}$$

It is the quantity generally represented by μ (Doran, 1995).

3.3.4. Specific water production rate

In the respiratory chain, there is an empirical relation between the rate of O_2 consumption and the production of H_2O:

$$q_{H_2O}^c = \gamma_{H_2O} q_{O_2}^c \tag{3.13}$$

Table 7 gives the values of this estimation.

3.3.5. Specific hydrogen consumption rate

With scheme

$$O_2 + 4H \rightarrow 2H_2O \tag{3.14}$$

the following relation applies

$$q_H^c = \rho_{H,O_2} q_{O_2}^c. \tag{3.15}$$

The mass coefficient ratio (equal to 0.125) then permits to calculate the specific hydrogen consumption rate associated with the oxygen uptake for water production.

Note: If all oxygen were consumed to produce water, the empirical constant γ_{H_2O} would be equal to the mass coefficient, ρ_{H_2O,O_2}, which is 1.125. Instead of this value, one finds 0.90 (see Table 7), which means that approximately 80% of the oxygen is used for water production. The 20% left are thus used to form oxygenated compounds of another nature. (One obviously thinks, inter alia, to the nitrogen oxidation, not measured in the experiments of Rieger et al.). Scheme (3.14) is thus incomplete and can be used only for hydrogen.

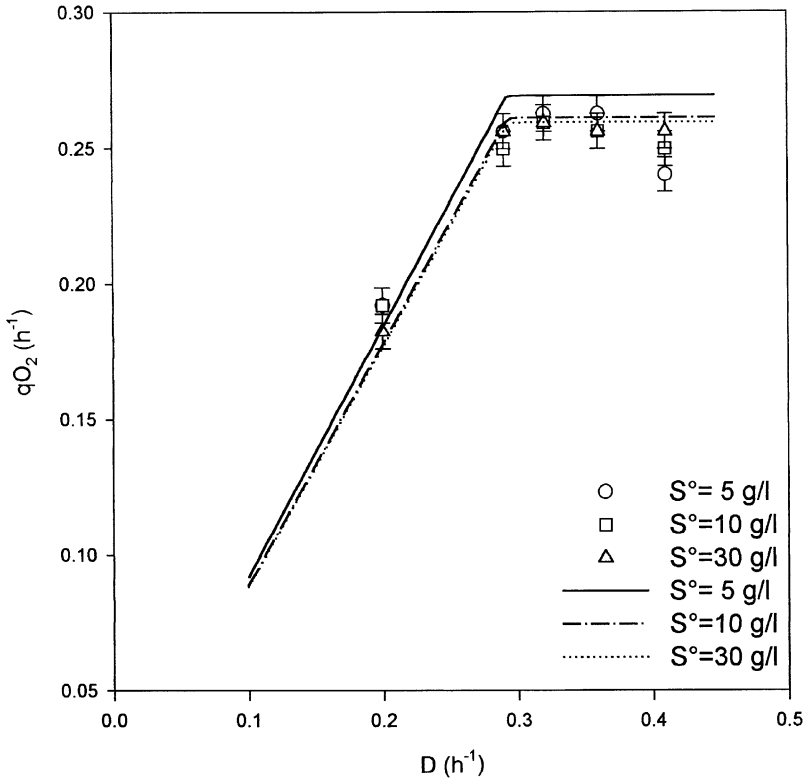

Fig. 7. Specific O_2 consumption rate profiles for the three feed concentrations. *Method*: Simulations were carried out by using the quantities derived from algorithm (2.24) and parameters of Table 1, with a substrate representation according to the EXP method. $S^0 = 5$ g/l: open circle: experimental data; full line: simulation. $S^0 = 10\,g/l$: open square: experimental data; dash-dotted line: simulation. $S^0 = 30$ g/l: open triangle: experimental data; dotted line: simulation. The specific rate was calculated according to relation (3.11). *Comments*: a slight dependence of the values at the plateau ($D > D_c$) with the feed substrate seems to appear. This effect is however very weak and the curves could be regarded as confused (see text and Table 6).

Table 7
Values of γ_{H_2O}

S^0 (g/l)	γ_{H_2O}
5	0.89
10	0.90
30	0.90

3.3.6. Specific respiratory CO_2 production rate

The specific rates conservation principle enables us to write that (cf. Fig. 6)

$$q^c_{CO_2(r)} = q^c_{GLU}(h) + \beta q^c_{GLU}(l) + q^c_{O_2} + q^c_H - (q^c_{H_2O} + q^c_{X/c}). \quad (3.16)$$

This relation allows deducing the specific production rate of respiratory CO_2 from the other rates. Fig. 8 shows good agreement between specific total CO_2 production rate and values calculated via Eqs. (3.7) and (3.13) ($CO_2(f) + CO_2(r)$). This agreement justifies the mode of calculation of $q^c_{CO_2(r)}$ and also all other rates necessary to calculate this one.

Fig. 9 shows the specific rates values just before the critical dilution rate ($D = 0.28\,h^{-1}$; upper (bold) values) and just after ($D = 0.32\,h^{-1}$; lower (italic) values). Transition between the respiratory and the respirofermentative mode is evident. It is also easy to verify that the specific rates are preserved and that the input specific rates balance matches the output specific rates balance. This verification can be globally done both on the whole diagram or according to the main specific ways (braces).

3.4. Molecular and elementary mass balance checking

Rieger et al. (1983) determined the elementary composition of the biomass and obtained the following balance:

$$C_6H_{12}O_6 + \alpha_1 O_2 + \alpha_2 0.15 NH_3 \rightarrow \alpha_2 CH_{1.79}O_{0.57}N_{0.15} + \alpha_3 C_2H_6O + \alpha_4 CO_2 + \alpha_5 H_2O. \quad (3.17)$$

They were able to calculate the values of the various stoichiometric coefficients for the experimental values of D. (Note that the nitrogen, for which experimental data are lacking, is eliminated in Eq. (3.17).) We can use these results to verify, by a completely independent method, if the various specific rates we calculated (and the model,

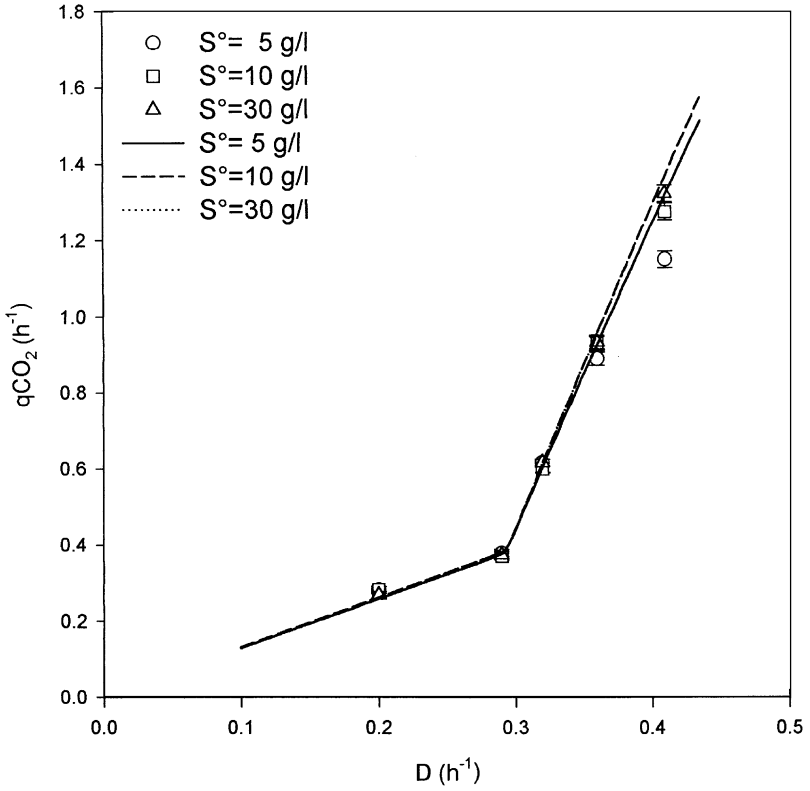

Fig. 8. Specific total CO_2 production rate profiles for the three feed concentrations. *Method*: as in Fig. 7. The total specific rate (respiratory + fermentation) was calculated by summing relations (3.7) and (3.16). *Comments*: The three curves are confused and the dispersion of mean experimental values increases with D. It should be noticed that there is no increase in the CO_2 production rate for $D > 0.32\,h^{-1}$ for the $S^0 = 30\,g/l$ profile. This seems contradictory to the significant increase in ethanol concentration for these dilution rates (see Fig. 3).

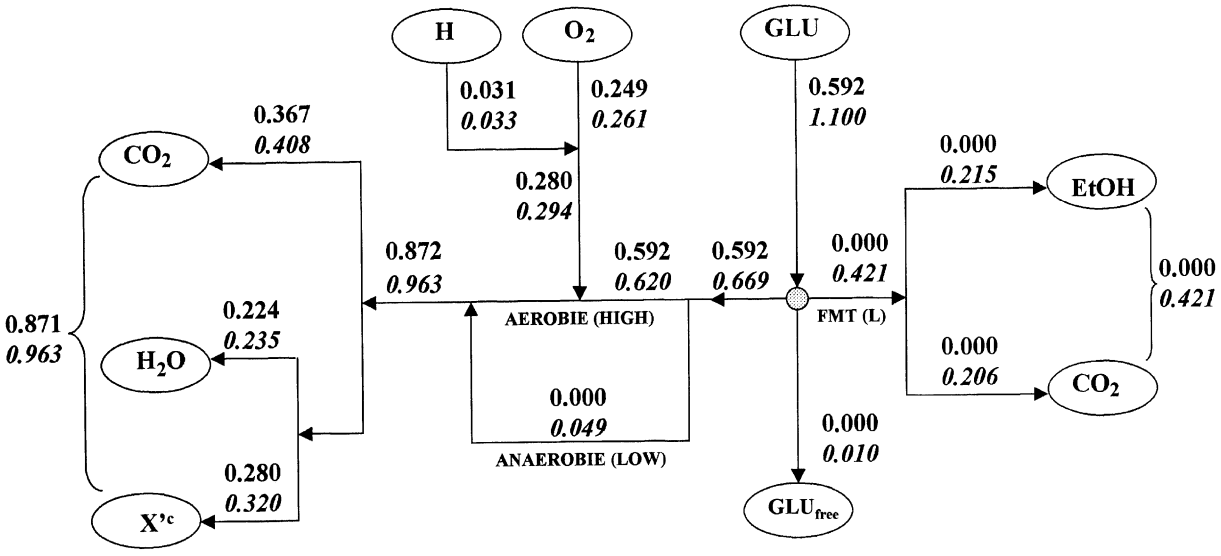

Fig. 9. Main specific rates quantification within the cellular phase. *Method*: Calculations were carried out with the kinetic parameters of Table 1 and residual substrate was evaluated according to the EXP method. The feed concentration is $S^0 = 10\,g/l$. *Comment*: This figure shows numerical values corresponding to the diagram of Fig. 6. The values have been calculated just before and just after the critical value $D_c = 0.3\,h^{-1}$. The upper (bold) value corresponds to $D = 0.28\,h^{-1}$; the lower (italic) value to $D = 0.32\,h^{-1}$. It is noted that specific rates: ANAEROBIC (LOW), fermentation (FMT(L)), as well as the free substrate way (adsorbed and/or intracellular) are zero before the critical value ($0.3\,h^{-1}$). Specific rates conservation principle can be verified on the whole diagram (sum of inputs = sum of outputs) or partially (braces). To calculate the metabolic flux, one just needs to multiply the specific rates values by the biomass ($X^{/c}$) at the corresponding dilution rate (data not shown).

in general), also agree with the elementary balance (3.17). It is enough for us to check if our stoichiometric coefficients values are comparable with those of the authors. Thereafter, we will use a biomass molecular weight equal to that appearing in Eq. (3.17), that is to say 25 g.

Using (2.26) and (2.28), we can show that

$$v_{Pi} = \frac{q^c_{Pi}}{MM_i}\frac{v_S MM_S}{q^c_S}, \tag{3.18}$$

where $v_j$and MM_j are the stoichiometric coefficients and the molar mass of compound j.

In the particular case (3.17), this becomes

$$v_{Pi} = \frac{q^c_{Pi}}{MM_i}\frac{180}{q^c_{GLU}(E)} \tag{3.19}$$

with $q^c_{GLU}(E) = \Phi^0_{GLU}/X^{/c}$, the specific interphasic exchange rate (*SIER*) (this term account for the totality of the glucose implied in reaction (3.17), which excludes residual glucose in the chemostat). This relation allows calculating all the stoichiometric coefficients and thus also the molecular and elementary mass balance (3.17), provided that $MM_{X/c}$ is known. Table 8 shows the comparison between the coefficients obtained in

Table 8
Calculation of stoichiometric coefficient (based on EXP procedure for residual substrate computation)

$C_6H_{12}O_6 + c_1 \cdot O_2 + c_2 \cdot 0.15 \cdot NH_3 \rightarrow c_2 \cdot CH_{1.79}O_{0.57}N_{0.15} + c_3 \cdot C_2H_60 + c_4 \cdot CO_2 + c_5 \cdot H_2O$										
D (h^{-1})	S^0 (g/l)		c_1	c_2	c_3	c_4	c_4 *resp*	c_4 *fer*	c_5	MB (%)
0.2	5	α	2.53	3.30	0.00	2.70	—	—	3.79	
		v	2.48	3.46	0.00	2.55	2.55	0	3.92	−0.4
	10	α	2.52	3.31	0.00	2.69	—	—	3.78	
		v	2.37	3.41	0.00	2.54	2.54	0	3.79	−0.3
	30	α	2.45	3.38	0.00	2.62	—	—	3.74	
		v	2.35	3.41	0.00	2.54	2.54	0	3.76	−0.2
0.29	5	α	2.41	3.42	0.00	2.58	—	—	3.71	
		v	2.47	3.44	0.00	2.55	2.55	0	3.91	−0.4
	10	α	2.37	3.46	0.00	2.54	—	—	3.68	
		v	2.36	3.40	0.00	2.54	2.54	0	3.77	−0.3
	30	α	2.41	3.42	0.00	2.58	—	—	3.71	
		v	2.34	3.40	0.00	2.53	2.53	0	3.75	−0.3
0.32	5	α	1.33	2.04	0.84	2.28	—	—	2.11	
		v	1.40	2.13	0.76	2.29	1.52	0.77	2.21	0.6
	10	α	1.34	2.08	0.83	2.20	—	—	2.12	
		v	1.33	2.09	0.77	2.28	1.51	0.77	2.13	0.7
	30	α	1.33	2.05	0.84	2.27	—	—	2.11	
		v	1.32	2.09	0.77	2.28	1.51	0.77	2.12	0.7
0.36	5	α	0.87	1.50	1.18	2.13	—	—	1.45	
		v	0.85	1.46	1.13	2.14	1.01	1.13	1.35	2.0
	10	α	0.80	1.41	1.24	2.11	—	—	1.34	
		v	0.80	1.42	1.14	2.13	0.99	1.14	1.28	2.1
	30	α	0.80	1.41	1.24	2.11	—	—	1.34	
		v	0.80	1.42	1.14	2.13	0.99	1.14	1.27	2.1
0.41	5	α	0.59	1.26	1.35	2.50	—	—	1.01	
		v	0.57	1.12	1.30	2.04	0.74	1.30	0.91	3.7
	10	α	0.55	1.13	1.42	2.03	—	—	0.98	
		v	0.53	1.08	1.32	2.03	0.72	1.32	0.86	3.8
	30	α	0.54	1.09	1.44	2.03	—	—	0.95	
		v	0.53	1.08	1.32	2.03	0.72	1.32	0.85	3.8

experiments by Rieger et al. (α) and those calculated by Eq. (3.19) (v). The $\boldsymbol{c_j}$ values at the head of the columns indicate the indices of the coefficients as they appear in Eq. (3.17). The column on the right (MB) shows the departure (in percent) from the exact mass balance. Our approach gives the possibility to differentiate the stoichiometric coefficients of respiratory CO_2 ($v_4(resp)$) from respirofermentative CO_2 ($v_4(fer)$) and obviously $v_4 = v_4(resp) + v_4(fer)$.

One the whole the comparison between the two sets of results shows a good agreement and the mass recovery is always higher than 96%, which is perfectly compatible with experimental data. It should, however, be noted that difference in mass recovery slightly increases according to D, which probably indicates a small systematic bias. This bias could be explained by the oversimplification of the process representation (3.17) and in particular by the absence of data concerning nitrogen flux, which account for 8% of the biomass; another cause could come from the absence of free glucose in Eq. (3.17), in which case it would be necessary to bring a corrective term to (3.19). Departure from "ideality" is too low and experimental data are insufficient to justify a relevant correction and one can admit that the obtained results are satisfactory.

3.5. Approximate relation for metabolites excretion

We give here a simplified approximate relation that allows to easily calculate the metabolite concentration in the matric phase without having computing all the specific rates. Part of the parametric estimation process is thus avoided and the method can easily be carried out manually by use of experimental data $\{S, X^{/c}\}$ and yield coefficient, Y_M (obtained for $D<D_c$). However, the method is only applicable if free glucose in cellular phase is low. The interest of the method rests on the fact of being able as to estimate the theoretical production of a metabolite produced by homo-fermentation, without having to measure it directly and to ensure that the process is rather homofermentative. The discussion of the applications comes out of the framework of this work.

We previously showed that

$$\frac{X^{/c}}{X^c} = \frac{q_S^c(h) + \beta q_S^c(l)}{q_S^c(h) + q_S^c(l)} \leqslant 1, \tag{3.20}$$

This relation then permits to calculate the difference $X^c - X^{/c} \geqslant 0$:

$$X^c - X^{/c} = \frac{X^c}{q_S^c(h) + q_S^c(l)}(1-\beta)q_S^c(l). \tag{3.21}$$

When $\tilde{C}_S^c \ll 1$, the specific rates conservation principle (in substrate-equivalent) can be approximated by the following relation (cf. Fig. 6)

$$q_S^c(h) + q_S^c(l) \approx \frac{\Phi_S^0}{X^{/c}}. \tag{3.22}$$

Putting this value in Eq. (3.21) leads to

$$X^c - X^{/c} = \frac{X^c}{\Phi_S^0} X^{/c}(1-\beta)q_S^c(l). \tag{3.23}$$

Multiplying the left- and the right-hand side by the mass coefficient ratio of metabolite P_i and comparing with the right-hand side with (2.31), it is obvious that

$$\tilde{C}_{Pi}^m = (X^c - X^{/c})\frac{\rho_{Pi,S}}{Y_M} \tag{3.24}$$

X^c can be calculated starting from experimental data as in algorithm (2.24) ($X^c = Y_M(S^0 - S)$). For any experimental value $X_{\exp} = X^{/c}$ it is then possible to calculate the concentration of the metabolite P_i (provided that the biomass is not too high).

We have compared the relationship (3.24) to the rigorous methods used previously. Let us define

$$\theta_{Pi} = \frac{\rho_{Pi,GLU}}{Y_M}, \quad P_i = EtOH, CO_2. \tag{3.25}$$

Fittings obtained by the experimental method (EXP) and by the generator model (GM) method give the same results for all the feed concentrations. Comparison between rigorous methods and approximate relation (3.25) is given in Table 9 (the value of θ in Eq. (3.25) was obtained by manual adjustment associated with a least-squares calculation so that $P_i(D)$ is as close as possible to rigorous adjustments).

It is obvious that the simple estimation (3.24) provides results completely comparable with those obtained by the complete model. It is doubtful that a more rigorous parametric estimation procedure will radically change this conclusion.

Table 9
Comparison of rigorous methods and approximation (3.25)

S^0 (g/l)	θ_{EtOH} (EXP,GM)	θ_{EtOH} (3.25)	θ_{CO_2} (EXP,GM)	θ_{CO_2} (3.25)
5	1.05	1.06	1.00	1.02
10	1.05	1.08	1.00	1.03
30	1.05	1.08	1.00	1.03

4. Discussion

Several types of models devoted to metabolic flux calculation use optimization criteria as constraint in order to solve an underdetermined set of equations. These criteria are often based on very general principles, frequently not decisively validated. In fact, they are often hypothesis based on concepts related to the biological theory of evolution. Among these criteria,

the growth rate maximization appears on many occasions (Varma and Palsson, 1993, 1994; Bellgardt, 2000b; Giusepin and van Riel, 2000). In a chemostat, this criterion cannot be used for the growth rate is dictated by the external conditions of the culture: specific growth rate is not maximum but equal to the dilution rate ($\mu = D$). Obviously, this relation can be used as a constraint, but it is relevant at a global level of description, which is poorly adapted to metabolic flux calculations. Our approach makes it possible to highlight an optimization criterion that applies under some particular conditions.

Let us define the specific metabolization rate by (see Fig. 6)

$$q_S^c(met) = q_S^c(h) + \beta q_S^c(l). \tag{4.1}$$

This rate characterizes all the anabolism processes (biosynthesis) and associated fueling reactions.

Moreover, the specific interphasic exchange rate (*SIER*) corresponds to the net total rate of substrate-equivalent flowing through the cellular phase:

$$SIER = q_S^c(h) + q_S^c(l) + q_S^c(free) = \frac{\Phi_S^0}{X^{/c}}, \tag{4.2}$$

where $q_S^c(free)$ is the specific rate of free (not metabolized) substrate. The ratio between the specific metabolization rate and the total specific rate is then given by

$$\frac{q_S^c(met)}{SIER} = \frac{q_S^c(h) + \beta q_S^c(l)}{q_S^c(h) + q_S^c(l) + q_S^c(free)}. \tag{4.3}$$

Before the transition ($D < D_c$), $q_S^c(l) = q_S^c(free) = 0$ and thus

$$q_S^c(met) = SIER = \frac{D}{Y_M}. \tag{4.4}$$

The metabolization rate is then maximum. After the transition, if $q_S^c(free)$ is negligible in front of the other specific rates, (4.3) becomes

$$\frac{q_S^c(met)}{SIER} = \frac{q_S^c(h) + \beta q_S^c(l)}{q_S^c(h) + q_S^c(l)}. \tag{4.5}$$

We previously showed that

$$X^{/c} = \frac{q_S^c(h) + \beta q_S^c(l)}{q_S^c(h) + q_S^c(l)} X^c. \tag{4.6}$$

Using this relation and (4.2), relation (4.5) becomes

$$\frac{q_S^c(met)}{\Phi_S^0} = \frac{1}{X^c}. \tag{4.7}$$

Rearranging and using the definition of the yield coefficient, one obtains finally that

$$q_S^c(met) = \frac{D}{Y_M} \tag{4.8}$$

i.e. the same value as Eq. (4.4). In other words, the metabolization rate keeps its maximum value both in respiratory and in respirofermentative mode as well, provided that the low-affinity pathway is able (k_0^* large) to treat enough substrate so that the free intracellular substrate concentration is low. It is indeed what occurs in the example of Rieger et al. that we have treated. For any underdetermined metabolic flux analysis relating to systems of this type, the relevant constraint would not be the growth rate maximization but the net specific metabolization rate (or flux) maximization. After the transition, there is a surplus specific "rate"

$$q_S^c(exc) = \frac{\Phi_S^0}{X^{/c}} - \frac{D}{Y_M} \tag{4.9}$$

which corresponds to the specific metabolites excretion rate (ethanol and fermentative CO_2). If excretion of metabolites exists, it is obvious that the transport capacity of the substrate must exceed the maximum metabolization rate. This comes together with the observations of Van Urk et al. (1989). The model does not allow to know if the transport of the surplus substrate is controlled so that excreted flux is adapted to maximum of metabolization (to ensure a redox balance, for example) or if, on the contrary, the metabolization rate acts as a bottleneck which obliges the excretion of a surplus of substrate that the cell cannot avoid. This last interpretation means that the uncontrolled substrate entrance would allow glucose to be used as a "signal" for (a) saturating the high-affinity pathway and (b) triggering the low-affinity pathway. This signal would have a purely kinetic effect, since when its concentration increases (after the threshold), the hyperbolic form saturates whereas the first-order reaction becomes significant. The Crabtree effect could then be interpreted in term of competition of two metabolic pathways controlled by the substrate. There are arguments supporting a regulation of substrate transport (Lagunas et al., 1982; Carlson, 1987; Van Urk et al., 1989; Lagunas, 1993). However, to our knowledge, it is not possible, to date, to assert that this regulation is always effective for all the transport systems of a strain (Walsh et al., 1996). Recent studies (Cortassa et al., 1997, 1998) seem to confirm our approach of a substrate regulation both at metabolization and at transport level.

An interesting remark can still be inferred from (4.4) and (4.8). Combining (3.12) with one of these relations, one shows easily that

$$\frac{q_{X/c}^c}{q_S^c(met)} = Y_M. \tag{4.10}$$

This relation shows that the relationship between the specific biomass production rate (or flux) and the specific metabolization (biosynthesis + fueling) rate (or flux), expressed in substrate-equivalent, is constant before and after the transition. Moreover, this value is the same as Y_M, the "yield coefficient" of the generator model. However, this value is not the true yield coefficient of the system and we propose to call it the

biosynthesis efficiency coefficient. This coefficient can be regarded as a measure of the coupling between the biosynthesis flux and the associated fueling flux. The discussion comes out of the framework of this work but the value obtained in this particular case shows that the coupling between the two pathways (expressed in substrate-equivalent) remains invariant and is with its maximum value both in respiratory and in respirofermentative mode. To conclude, the example of the Crabtree effect in *S. cerevisiae* shows that a model with two transport/metabolization pathways, with high and low affinity, allows to account for the main properties of an abrupt transition from respiratory to respirofermentative mode, in the case of a homofermentative production of ethanol. Kinetics very similar to the local form of Eq. (2.9) was used effectively by Walsh et al. (1994) to describe the glucose transport rate in the wild-type X-2180 *S. cerevisiae* strain cultivated in batch. The low-affinity component (not saturable or of first-order) was interpreted by the authors as a simple diffusion term. Moreover, using a two ways model, they noted that the affinity for glucose decreases when the biomass increases. The data are insufficient to check if the product of the half-saturation constant by the biomass is constant, but the variation of the affinity observed by the authors goes well in the same direction as the one given by the total affinity ($K_S^* X^{/c}$) appearing in Eq. (2.9). These results considerably reinforce the idea that the non-local representation is justified. From the modeling point of view, we have shown that the kinetic parameters could be considered as true constants on the whole dilution rates interval and for the three concentrations in the feed of the chemostat. The model is of great simplicity and does not require any prerequisite, like optimization criteria or logical test, to calculate the algorithm. Hyperbolic form of the kinetics reflects well the transport phenomenon by diffusion or facilitated diffusion, which characterizes the transport of glucose in *S. cerevisiae* (Schechter, 1997; Walker, 1998). The stoichiometric mass balance confirms, by use of an independent method, the validity of the mass balances for the PDS.

Our representation rests explicitly on the fact that the whole of the process is controlled by substrate interphasic exchanges phenomena and on the intracellular metabolization of this one. In particular, the specific oxygen uptake rate is deduced from the metabolic high-affinity pathway. This allows to give a correct account of the specific rate of O_2, and also to verify the stoichiometry of the reaction. These results plead in favor of an explanation of the Crabtree effect based on glucose metabolization and transport and not on the limitation of the respiratory chains capacity (Sonnleitner and Käpelli, 1986). Different arguments going in the same direction can be found in Walker (1998) and Aon and Cortasssa (2001). From the biotechnology point of view, we think that the kinetic parameters of the model allow to characterize quantitatively a particular strain engaged in a specific process. One could thus, for example, quantify the effects of a genetic modification or evaluate the impact of a culture medium modification. In particular, the relation relating critical dilution rate to intrinsic and global characters of a culture ($D_c = V_S^0 Y_M$) could be used as "guideline" for the optimization of processes aiming at preferentially producing biomass (like baker's yeast) or, on the contrary, metabolites (like ethanol) in fermentations industry. Cortassa and Aon (1998), for example, showed that the value of D_c could vary according to mutants carrying glucose-repressible genes disruptions. In this study, it appeared that all mutants displayed a critical dilution rate and a maximum T/M specific rate lower than those of the wild strain. Except for one mutant (*snf4*), all the yield coefficients were also lower. This last example shows that it is possible, by modifying a gene, to preserve a global quantity, like the yield coefficient, while modifying local properties (like the high-affinity T/M maximum specific rate; in case of *snf4,* reduction was about 25%). Conversely, it is also possible to change global and local parameters simultaneously. Our approach allows easily quantifying this kind of modification and provides thus a characterization tool for evaluation and optimization of processes.

References

Aon, J.C., Cortassa, S., 2001. Involvement of nitrogen metabolism in the triggering of ethanol fermentation in aerobic chemostat cultures of *Saccharomyces cerevisiae*. Metab. Eng. 3, 250–264 doi: 10.1006/mben.2001.0181.

Barford, J.P., Hall, R.J., 1979. An examination of the Crabtree effect in *Saccharomyces cerevisiae*: the role of the respiratory adaptation. J. General Microbiol. 114, 267–275.

Barford, J.P., Jeffrey, P.M., Hall, R.J., 1981. The Crabtree effect in *Saccharomyces cerevisiae*—primary control mechanism or transient. In: Moo-Young, M. (Ed.), Advances in Biotechnology 1. Pergamon Press, Englewwod Cliffs, NJ, pp. 255–260.

Bellgardt, K.H., 2000a. Baker's yeast production. In: Schügerl, K., Bellgardt, K.H. (Eds.), Bioreaction Engineering. Springer Verlag, Berlin, Heidelberg, pp. 277–320.

Bellgardt, K.H., 2000b. Bioprocess models. In: Schügerl, K., Bellgardt, K.H. (Eds.), Bioreaction Engineering. Springer Verlag, Berlin, Heidelberg, pp. 21–41.

Carlson, M., 1987. Minireview: regulation of sugar utilization in *Saccharomyces* species. J. Bacteriol. 169, 4873–4877.

Cortassa, S., Aon, M.A, 1997. Distributed control of the glycolytic flux in wild-type cells and catabolite repression mutants of *Saccharomyces cerevisiae* growing in carbon-limited chemostat cultures. Enz. Microbiol. Technol. 21, 596–602.

Cortassa, S., Aon, M.A., 1998. The onset of fermentative metabolism in continuous cultures depends on the catabolite repression properties of *Saccharomyces cerevisiae*. Enz. Microbiol. Technol. 22, 705–712.

Crabtree, H.G., 1929. Observations on the carbohydrate metabolism of tumours. Biochem. J. 23, 536–545.

D'Amore, T., Panchal, C.J., Stemart, G.G., 1988. Intracellular ethanol accumulation in *Saccharomyces cerevisiae* during fermentation. Appl. Environ. Microbiol. 54, 110–114.

De Deken, R.H., 1966. The Crabtree effect. A regulatory system in yeast. J. Gen. Microbiol. 44, 149–156.

Doran, P.M., 1995. Bioprocess engineering principles. Academic Press, London.

Guijarro, J.M., Lagunas, R., 1984. *Saccharomyces cerevisiae* does not accumulate ethanol against concentration gradient. J. Bacteriol. 60, 874–878.

Giusepin, M.L., van Riel, N.A.W., 2000. Metabolic modeling of *Saccharomyces cerevisiae* using the optimal control of homeostasis: a cybernetic model definition. Metab. Eng. 2, 14–33 doi: ID mben.1999.0134.

Lagunas, R., 1993. Sugar transport in *Saccharomyces cerevisiae*. FEMS Microbiol. Rev. 104, 229–242.

Lagunas, R., Dominguez, C., Busturia, A., Sáez, M.J., 1982. Mechanisms of appearance of the Pasteur effect in *Saccharomyces cerevisiae*: inactivation of sugar transport systems. J. Bacteriol. 152, 19–25.

Nielsen, J., Villadsen, J., 1994. Bioreaction engineering principles. Plenum Press, New York.

Postma, E., Scheffers, W.A., van Dijken, J.P., 1989. Kinetics of growth and sugar transport in glucose-limited chemostat culture of *Saccharomyces cerevisiae* CBS 8066. Yeast 5, 159–165.

Rieger, M., Käpelli, O., Fiechter, A., 1983. The role of limited respiration in the complete oxidation of glucose by *Saccharomyces cerevisiae*. J. General Microbiol. 129, 653–661.

Roels, J.A., 1983. Energetics and Kinetics in Biotechnology. Elsevier Biomedical Press, The Netherlands.

Schechter, E., 1997. Biochimie et Biophysique des Membranes—Aspects Structuraux et fonctionnels. Masson, Paris.

Sonnleitner, B., Käpelli, O., 1986. Growth of *Saccharomyces cerevisiae* is controlled by its limited respiratory capacity: formulation and verification of a hypothesis. Biotechnol. Bioeng. 28, 927–937.

Thierie, J., 1997. Why does bacterial composition change with the chemostat dilution rate? Biotechnol. Tech. 11, 625–629.

Thierie, J., 2000. Cellular cycling of substrate as a possible cryptic way for energy spilling in suspended cellular continuous cultures. Biotechnol. Lett. 22, 1143–1149.

Van Urk, H., Postma, E., Scheffers, W.A., Van Dijken, J.P., 1989. Glucose transport in Crabtree-positive and Crabtree-negative yeasts. J. General Microbiol. 135, 2399–2406.

Varma, A., Palsson, B.O., 1993. Metabolic capabilities of *Escherischia coli*. II. Optimal growth pattern. J. Theor. Biol. 165, 503–522.

Varma, A., Palsson, B.O., 1994. Stoichiometric flux balance models quantitatively predicts growth and metabolic by-products secretion in wild-type *Escherischia coli* W3110. Appl. Environ. Microbiol. 60, 3724–3731.

von Meyenburg, H.K., 1969. Katabolit-Repression und der Sprossung zyklus von *Saccharomyces cerevisiae*. Ph.D. thesis, Eidgenössische Technsiche Hochshulle, Zürich.

Walker, G.M., 1998. Yeast—Physiology and Biotechnology. Wiley, Chichester, England.

Walsh, M.C., Smits, H.P., Scholte, M., van Dam, K., 1994. Affinity of glucose transport in *Saccharomyces cerevisiae* is modulated during growth on glucose. J. Bacteriol. 176, 953–958.

Walsh, M.C., Scholte, M., Valkier, J., Smits, P., van Dam, K., 1996. Glucose sensing and signaling properties in *Saccharomyces cerevisiae* require the presence of at least two members of the glucose transporter family. J Bacteriol. 178, 2593–2597.

Wojtczak, L., 1996. The Crabtree effect: a new look to the old problem. Acta. Biochim. Pol. 43, 361–368.